Electronic structure and Fermi surface of Sn/Cu(100)-$(3\sqrt{2}\times\sqrt{2})R45°$

J. Martínez-Blanco,[1] V. Joco,[1] J. Fujii,[2] P. Segovia,[1] and E. G. Michel[1]
[1]*Departamento de Física de la Materia Condensada and Instituto Universitario de Ciencia de Materiales "Nicolás Cabrera," Universidad Autónoma de Madrid, 28049 Madrid, Spain*
[2]*TASC National Laboratory, CNR-INFM, S.S. 14, km 163.5, I-34012 Trieste, Italy*
(Received 1 February 2008; revised manuscript received 16 April 2008; published 14 May 2008)

The surface phase Sn/Cu(100)-$(3\sqrt{2}\times\sqrt{2})R45°$ exhibits a temperature induced phase transition to a $(\sqrt{2}\times\sqrt{2})R45°$ phase above 360 K. We report an angle-resolved photoemission study of the two-dimensional Fermi surface of the low-temperature phase. The Fermi surface is formed by folding of a quasi-two-dimensional surface band and presents three contours. It is characterized by gaps appearing in optimally nested regions of one of the contours, whereas other sections remain ungapped. We address the origin of the folding and of the surface phase transition, which is attributed to the formation of a surface charge density wave.

DOI: 10.1103/PhysRevB.77.195418 PACS number(s): 73.20.At, 68.35.Rh

I. INTRODUCTION

Low dimensional materials exhibit a broad range of physical phenomena with specific properties. Phase transitions are an important example of rich new phenomenology related to low dimensionality. We may mention within this broad field metal-insulator transitions,[1] superconductivity,[2] ferroelectricity,[3] and charge density waves (CDWs).[4,5] Two-dimensional (2D) phase transitions, where a CDW is possibly stabilized, have deserved ample attention and have been actively searched during recent years.[6–8] The reason is the interesting properties of the CDW collective state.[5] The CDW consists in a periodic lattice distortion of the surface lattice of spatial periodicity close to $2\pi/2k_F$. In a surface with partly filled electronic surface states, the electronic response function is maximum for the spanning or nesting vector $2k_F$. The maximum is enhanced by the presence of large parallel portions of the Fermi surface separated by $2k_F$ (nesting condition), simply because more electrons are coupled by the same $2k_F$ vector. The new periodicity opens a zone edge band gap, so that the outcome of this process is to eliminate in part the 2D Fermi surface. In the nested areas, new completely filled states appear, separated by a band gap $2W$ from empty states. Due to the lattice involvement, a large electron-phonon coupling is expected, which often comes along with a soft phonon. In this case, the dynamic of the phase transition between the normal and the CDW state is described by the freezing of the soft phonon as temperature decreases.

A first approach to investigate 2D CDWs is looking for three-dimensional systems with a low dimensional structure (such as layered compounds).[9] Another way is to investigate metal monolayers, whose electronic states can be directly probed by surface-sensitive techniques.[10] In this case, electrons characteristic of the surface or interface with the substrate are confined in a quasi-2D region. In metal-semiconductor interfaces, the metallic surface bands are naturally confined in the surface region. There have been quite a few candidates for surface CDWs, but the interpretation in terms of CDW stabilization has been often disputed.[7,11] On the other hand, metal-metal interfaces have also been considered, and several surface systems of this kind have also been proposed to represent a surface CDW.[12] In principle, electronic surface confinement is required, and thus surface electrons cannot mix with bulk states, either because there are bulk band gaps, or because of symmetry. These conditions (in particular, the surface confinement) are not always fulfilled, which makes the data interpretation less straightforward.

The most important feature of the CDW state is the electronic energy gain, related to the $2W$ gap opening. Due to this fact, a common way to understand the properties of a particular CDW system is to compare the size of the electronic gap with respect to the phonon energies. Tosatti[10] established some time ago a classification of surface charge density waves based on these ideas. In the weak-coupling limit, the electronic gap $2W$ is comparable to phonon energies, then the formation of the CDW tends to be a nonadiabatic phenomenon because when $k_BT\sim 2W$, the gap looses its reason for stability, and disappears at the critical temperature T_c, at the same time as the lattice distortion. The lattice plays a minor role in the transition, since it only follows the electronic distortion. We may say that in the weak-coupling limit, the CDW phase transition is governed by the electronic entropy. On the contrary, an electronic gap much larger than phonon energies (strong-coupling limit) indicates that a superlattice of new chemical bonds is formed in the CDW phase. As the electronic gap is much larger than k_BT, electron entropy is irrelevant, and the phase transition is driven by the lattice entropy. Due to this reason, the band gap survives up to a temperature T_0 that can be much larger than the critical temperature T_c. Each limit is characterized by a different CDW correlation length ξ_{CDW},[10,13] defined as the length scale of coherent lattice CDW ordering required to observe a CDW gap extending for δk in reciprocal space ($\xi_{\mathrm{CDW}}=2\pi/\delta k$). In the strong-coupling limit, ξ_{CDW} is comparable to the lattice spacing, and the CDW gap extends in the whole reciprocal space. In the weak-coupling limit, ξ_{CDW} is significantly larger, and the gap is observed only in a reduced portion of reciprocal space. Concerning the dynamic of the phase transition, due to the different behavior of the lattice with respect to the distortion, the weak-coupling limit usually corresponds to a displacive phase transition triggered at the critical temperature. In the strong-coupling limit, an order-disorder phase transition is observed at T_c. The CDW

long range order is lost, but small domains survive up to T_0, when the band gap is closed.

Recent findings show that ordered superstructures of group III and IV metals adsorbed on Cu(100) (and possibly other noble metals) exhibit features typical of both the strong- and weak-coupling limits. These results support the existence of a new paradigm, corresponding to systems in the strong-coupling limit but with a long coherence length ξ_{CDW}, as proposed by Aruga.[13] A common feature is the appearance of surface reconstructions of $(n\sqrt{2}\times m\sqrt{2})R45°$ type, where n and m are integer numbers for submonolayer metal coverages. Some of these reconstructions exhibit temperature induced phase transitions into a simpler $(\sqrt{2}\times\sqrt{2})R45°$ or sometimes into a $p(2\times2)$ structure at higher temperatures, which are accompanied by changes in the surface electronic structure. The appearance of surface band gaps concomitantly with the long range reversible phase transitions suggests that the stabilization of low-temperature phases is assisted by a surface charge density wave. The first observation of a surface band gap opening in this family of reconstructions corresponds to Tl/Cu(100)-$p(6\sqrt{2}\times2\sqrt{2})R45°$.[14] Later on, Nakagawa *et al.*[15–19] found that submonolayer amounts of In on Cu(100) surface form several ordered structures, and that three of them present reversible phase transitions upon heating, namely, $(9\sqrt{2}\times2\sqrt{2})R45°$ to $(\sqrt{2}\times\sqrt{2})R45°$, $(2\sqrt{2}\times2\sqrt{2})R45°$ to $p(2\times2)$, and $(\sqrt{20}\times\sqrt{20})R63.4°$ to $p(2\times2)$. In a previous work, we analyzed the case of Sn/Cu(100).[20] We showed that it is a prototypical interface, because for Sn/Cu(100) the nesting vector agrees very well with the periodicity of the low-temperature phase. In this scenario of excellent nesting, we expect that the role of the Fermi surface gapping is more important in the stabilization of the CDW phase.

Room temperature deposition of Sn on Cu(100) gives rise to a rich variety of surface reconstructions in the submonolayer coverage range. The phases observed at room temperature were reported some time ago,[21–23] and the phase diagram was reinterpreted more recently.[24] In a previous work, we reported a detailed investigation on the different phases appearing and their temperature stability range by using low-energy electron diffraction (LEED) and surface x-ray diffraction.[25] The unit cells have been imaged using scanning tunneling microscopy.[26] We summarize here the most important results and refer the reader to Ref. 25 for a more detailed account. A $p(2\times2)$ phase with split spots is observed at 0.2 ML, followed by a rotated domain $p(2\times6)$ at 0.33 ML. In the coverage range around 0.45 ML, a $\begin{pmatrix}-4 & 2\\ 0 & 4\end{pmatrix}$ phase is observed. A rotated domain $(3\sqrt{2}\times\sqrt{2})R45°$ ($3\sqrt{2}$ in the following) appears at 0.5 ML and a $(2\sqrt{2}\times2\sqrt{2})R45°$ phase at 0.65 ML. Two of these phases exhibit reversible phase transitions to a high-temperature phase, with a critical temperature close to 360 K in both cases. The $\begin{pmatrix}-4 & 2\\ 0 & 4\end{pmatrix}$ phase becomes $p(2\times2)$, while the $(3\sqrt{2})$ transforms into a $(\sqrt{2}\times\sqrt{2})R45°$ phase. The properties of this phase transition have been analyzed in Ref. 20. It was found that the surface phase transition is reversible, and that it is related to the opening of a large band gap at the Fermi level in the $(3\sqrt{2})$ phase. The band gap is observed in optimally nested regions of the Fermi surface, while areas with poorer nesting remain ungapped. This finding indicated that the $(3\sqrt{2})$ phase is stabilized by a gain in electronic energy, related with the Fermi energy gapping, and it can be understood as a CDW state.[13]

In this work, we report a detailed analysis of the Fermi surface of Sn/Cu(100)-$3\sqrt{2}$. The Fermi surface of Cu(100) has been also measured for the same experimental conditions, in order to discern the substrate contribution to the Fermi surface of Sn/Cu(100)-$3\sqrt{2}$. We discuss the topology of the Fermi surfaces and constant-energy surfaces and the origin of the features observed, and their role in the phase transition. We also analyze the changes induced by the formation of the surface CDW phase.

II. EXPERIMENT

Angle-resolved photoemission spectroscopy (ARPES) experiments were performed in two different ultrahigh vacuum (UHV) chambers. In the first one, He I radiation from a plasma source (Gammadata) excites valence band photoelectrons, which are detected using an ARUPS-10 electron analyzer. The energy resolution was set to 80 meV and the angle resolution was $\pm0.5°$. The second UHV chamber is located at the low-energy branch of the APE beamline, receiving synchrotron light from the Elettra storage ring in Trieste (Italy). Fermi surface mapping was performed at constant photon energy (27 eV), which was found to be the most favorable value due to restrictions from the bulk electronic structure. The surface and bulk bands were mapped in a window of approximately 4 eV below the Fermi energy using a Scienta electron analyzer. In this chamber, the polarization plane of the light was horizontal and coincided with the measuring plane. An energy window of 1.5 eV was mapped with high resolution in order to probe the electronic states closer to the Fermi energy. The energy resolution was set to 60 meV and the angle resolution was 0.12°. When photoemission intensity is represented in a gray scale, white corresponds to high intensity. Constant binding energy surfaces were mapped within approximately one-quarter of the reciprocal space, and were mirrored according to the fourfold symmetry of Cu(100). The Cu(100) sample was cleaned by Ar sputtering and annealing until a sharp (1×1) LEED pattern was observed. The quality of the surface was checked by measuring the narrow d-like surface state of odd symmetry at $\bar{M}$. The $3\sqrt{2}$ structure is produced by deposition of 0.5 ML of Sn at 300 K. The coverage is calibrated from the sequence of structures below 1 ML (Refs. 24 and 25) and from the Sn $5d$/Cu $3d$ intensity ratio measured with $h\nu=60$ eV. Symmetry points are referred to the Cu(100) surface Brillouin zone. k_x corresponds to $\bar{\Gamma}\bar{M}$ direction in this paper.

III. RESULTS

The electronic structure of Cu(100) is well known.[28] We comment here a few relevant features, which will be useful for the interpretation of the Sn/Cu(100) Fermi surface later. The electronic structure of noble metals near the Fermi energy is dominated by a single band of sp orbital origin, which is the only one crossing the Fermi energy and gener-

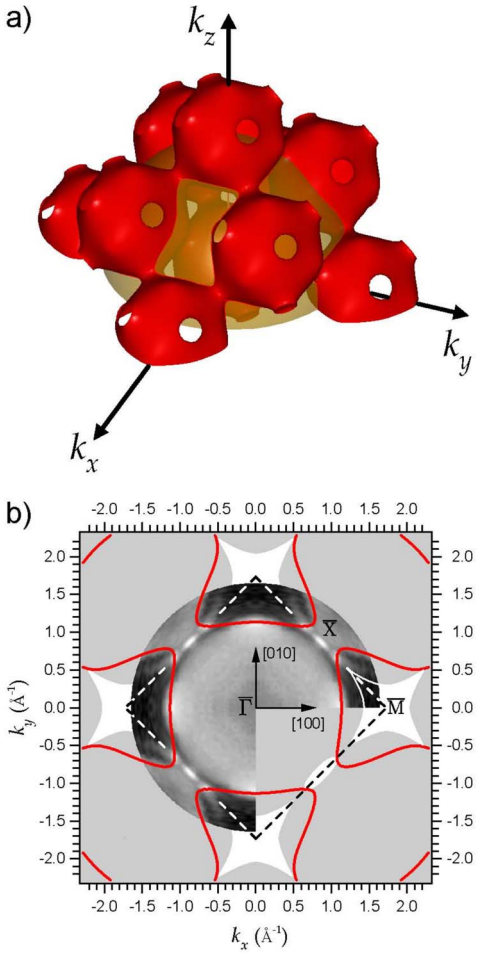

FIG. 1. (Color online) (a) The bulk Cu Fermi surface represented in the repeated zone scheme. The hemisphere corresponds to the wave vector of photoelectrons excited with $h\nu$=27 eV. (b) Fermi surface mapping for Cu(100) corresponding to $h\nu$=27 eV. The photoemission intensity is represented in a logarithmic gray scale. The (1×1) first Brillouin zone is drawn with dashed lines. White areas in the background correspond to absolute band gaps in the projection of the Cu bulk bands. The red (gray) lines represent the calculated Cu(100) bulk Fermi surface projection for the photon energy used (Ref. 27). The bulk band crossing is observed at this photon energy as an intensity increase along the $\overline{\Gamma M}$ direction coincident with the calculated Fermi surface. See text for information on additional features.

ating a Fermi surface of quasispherical shape. A hybridization band gap opens along ⟨111⟩ directions, giving rise to the necks joining neighboring Fermi surfaces in the repeated zone scheme in reciprocal space [see Fig. 1(a) for a three-dimensional picture]. The semitransparent hemisphere represents the distribution of initial states excited with the photon energy used in the experiment ($h\nu$=27 eV). Figure 1(b) (lower right quadrant) shows the projection of the bulk bands along the [001] direction. There is a large band gap around the $\bar{M}$ point and a smaller gap around the $\bar{X}$ point. Figure 1(b) shows the photoemission intensity for Cu(100) ($h\nu$=27 eV) in a narrow energy window of 25 meV around the Fermi energy. The image has not been subjected to any other treatment. Dashed lines represent the (1×1) first Brillouin zone. The red contours correspond to the bulk Fermi surface projection, calculated with a simple tight binding model[27] for $h\nu$=27 eV. The Fermi energy crossing by the *sp* band is observed as a high intensity close to the red contour at k_x=1.15 Å^{-1}. The crossing is shown in an energy vs parallel momentum representation in Fig. 2. There is a remarkable agreement between calculation and experiment. Note the intensity enhancement observed in the reciprocal space area between normal emission and the band crossing (occupied states side), which is due to the logarithmic scale used to represent the data.

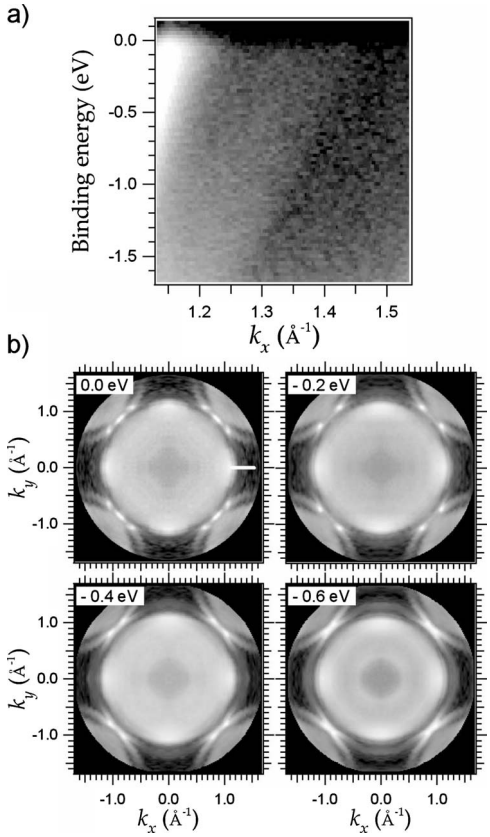

FIG. 2. (a) Binding energy vs parallel momentum along the $\overline{\Gamma M}$ direction for Cu(100) and $h\nu$=27 eV. The intense band crossing the Fermi level at ~1.15 Å^{-1} is the Cu bulk *sp* band. The diffuse intensity observed for $k_x \simeq 1.35$ Å^{-1} is due to the bulk band gap edge (see text). (b) Constant binding energy surfaces (photoemission intensity vs parallel momentum), measured with $h\nu$=27 eV for Cu(100) and for BE=0.0 (Fermi surface), 0.2, 0.4, and 0.6 eV. A white horizontal line highlights the area shown in panel (a). Photoemission intensity is represented in a logarithmic scale.

We note that for $h\nu$=27 eV, the *sp* band crossing does not correspond to the gap edge, which is defined by the maximum Fermi surface diameter perpendicular to the [100] direction (see Fig. 3). The gap edge is probed with photon energies around 45 eV. Due to the high density of states at the gap edge, transitions not conserving the momentum are observed as a weak, diffuse intensity right at the gap edge for different photon energies, including $h\nu$=27 eV (see Fig. 2). This observation agrees with previous findings[29] and theoretical calculations made within the framework of the one-step photoemission model,[30] which predict density of states indi-

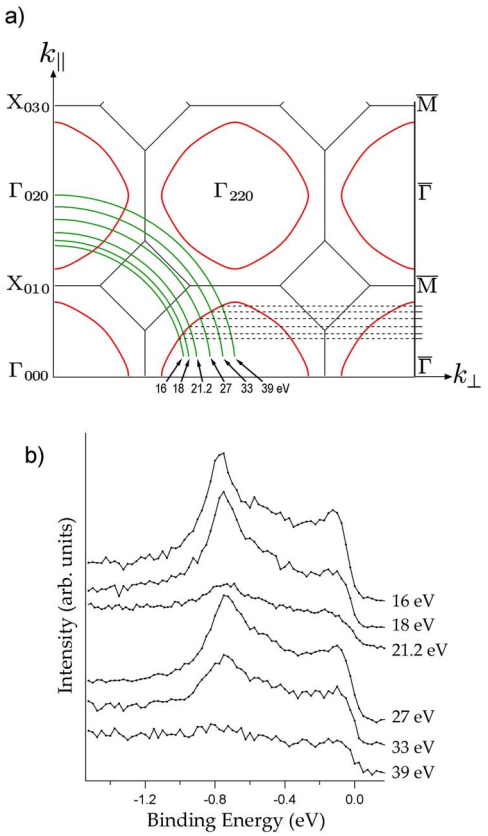

FIG. 3. (Color online) (a) Cu(100) reciprocal space scheme showing $k_{\perp}$ vs $k_{\|}$ along the $\bar{\Gamma}\bar{M}$ direction. Red lines (centered at $\bar{\Gamma}$ points) correspond to the cut of the bulk Cu Fermi surface and green lines (arcs centered at Γ_{000}) show the range of reciprocal space accessible (at the Fermi energy) for different photon energies. (b) Energy distribution curves for different photon energies taken for the $3\sqrt{2}$ phase of Sn/Cu(100) at $k_x \simeq 1.45$ Å^{-1} along $\bar{\Gamma}\bar{M}$.

rect transitions as those observed in Fig. 2. For a highly damped final state, an angle-resolved experiment directly measures the one-dimensional density of the initial states and consequently extremes in the band structure as a function of $k_{\perp}$ will induce features in the photoemission spectrum. Then, for an extremum crossing the Fermi energy, any feature representing a simple projection of the Fermi surface will be visualized in the photointensity. The intensity distribution in Fig. 1 is predominantly interpreted in terms of direct transitions, which reflect the crossing of the Fermi surface. However, less intense features corresponding to density-of-states-type transitions are also observed.

The intensity at $\bar{X}$ points corresponds to a Cu(100) surface state previously reported by Kevan.[31] This Shockley surface state lies in the projected bulk band gap between the bulk continuum edge and the Fermi level at $\bar{X}$, being highly localized in a small momentum and energy region. Due to its location near the Fermi energy, this surface state is more sensitive to contamination than other Cu surface states. Thus, a good visualization of this surface state is inherent to a well prepared surface.

Constant energy surfaces for binding energies down to 0.6 eV are shown in Fig. 2. The *sp* band crossing is detected at smaller parallel momentum values, as the binding energy increases, as expected from its parabolic dispersion. The diffuse contour around the gap edge reflects the Cu(100) Fermi surface cross section, when cut by a (001) plane passing through the zone center ($k_{\perp}=0$). The intense points around $\bar{X}$ correspond also to band extremes, in this case for $k_{\perp} \neq 0$.

The $(\sqrt{2}\times\sqrt{2})R45°$ structure appears above 360 K for 0.5 ML Sn deposited on Cu(100).[20,25] This phase exhibits a surface band *S* whose dispersion follows the Cu *sp* bulk band. In the following, we summarize its most important features, we refer the reader to Ref. 20 for more details. The surface band *S* is observed with high intensity in the gap around the $\bar{M}$ point, but also outside it. The dispersion of *S* along $\bar{\Gamma}\bar{M}$ follows a parabola with an effective mass $m^*=1.23$. The two Fermi energy crossings around the $\bar{M}$ point span a $2k_F$ vector equal to the periodicity required to stabilize the $(3\sqrt{2}\times\sqrt{2})R45°$ structure. Indeed, below 360 K, a two-domain $(3\sqrt{2}\times\sqrt{2})R45°$ phase is formed and a band gap opens at the precise location where the surface band *S* crossed the Fermi energy in the $(\sqrt{2}\times\sqrt{2})R45°$ structure. Since there are two 90°-rotated domains, only the zone edge of one domain is probed by ARPES, and thus two surface bands are detected, one coming from each rotated domain, but only one of them is backfolded at the $3\sqrt{2}$ zone edge. The two surface bands, related to the two $3\sqrt{2}$ domains, are shown in Fig. 3(b) for different photon energies and for $k_x \simeq 1.45$ Å^{-1}. Note the lack of dispersion with photon energy, as expected for a surface state. Figure 3(a) shows also a scheme of the bulk reciprocal space area probed for the different photon energies used. A photon energy of 27 eV was selected for most of the measurements. For this value of $h\nu$, the bulk band does not disperse too close to the Fermi energy, and there is a good angular resolution.

In order to characterize the changes in the electronic structure related to the CDW transition, we measured the Fermi surface of the $3\sqrt{2}$ structure. As mentioned above, due to the two-domain nature of the structure, there is always a band crossing the Fermi energy. Figure 4 shows an image of the Fermi surface, taken at 27 eV photon energy. Features *A* and *B* correspond to the *sp* Cu(100) band (see also Fig. 2). Feature *C* is visualized also in the clean sample and, as shown before, it is traced back to indirect transitions. The rest of the intensity observed is related to the surface states of the Sn induced superstructure. The Fermi surface has an apparently complex shape, but it can be easily rationalized if we realize that the main feature is a quasicircular contour centered at normal emission ($\bar{\Gamma}$ point), which contains the $(\sqrt{2}\times\sqrt{2})R45°$ Brillouin zone [Fig. 4(a)], and is due to the *S* surface state. The almost circular shape of the contour agrees well with the free-electron-like nature of *S*. All other features observed are simply interpreted after drawing this contour in the repeated zone scheme, as made in Fig. 4(a). The contour reproduced in the repeated zone scheme is obtained from a polynomial fit to the experimental Fermi contour. Once the opening of avoided-crossing band gaps is taken into account, the expected contours are modified as shown in Fig. 4(b). The contours reproduce the expected behavior for an ideal two-dimensional free-electron-like band, which has a Fermi momentum larger than the square surface Brillouin zone. The

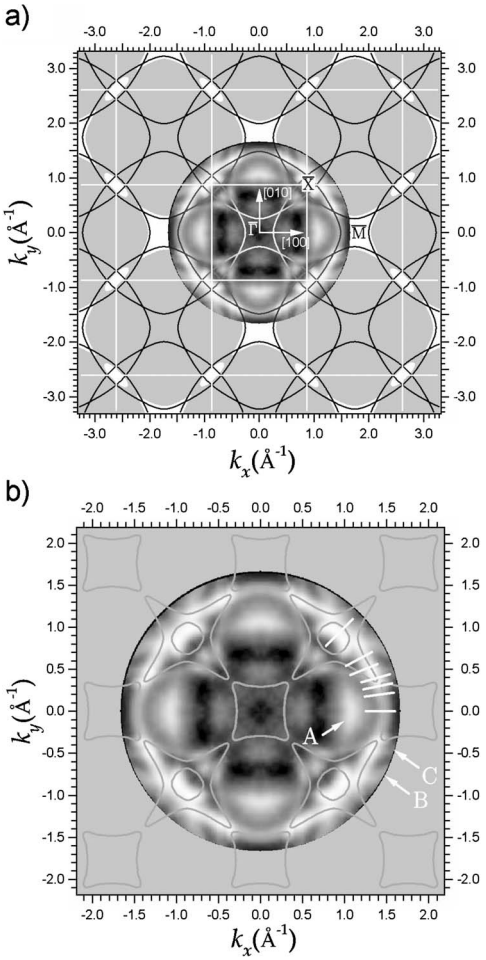

FIG. 4. Logarithm of the photoemission intensity integrated in an energy window of 25 meV around the Fermi level for Sn/Cu(100)-$3\sqrt{2}$ ($h\nu$=27 eV). (a) The gray background corresponds to the band bulk projection on the (100) face, leaving absolute gaps represented as white areas. White lines mark the $(\sqrt{2}\times\sqrt{2})R45°$ Brillouin zone edges. A black quasicircular line represents the surface state Fermi contour, which is repeated with $(\sqrt{2}\times\sqrt{2})R45°$ periodicity. (b) Same as (a), including the avoided-crossing band gaps in the surface state Fermi contour. Arrows *A*, *B*, and *C* highlight specific features (see text). Straight lines correspond to directions shown in Figs. 6 and 7.

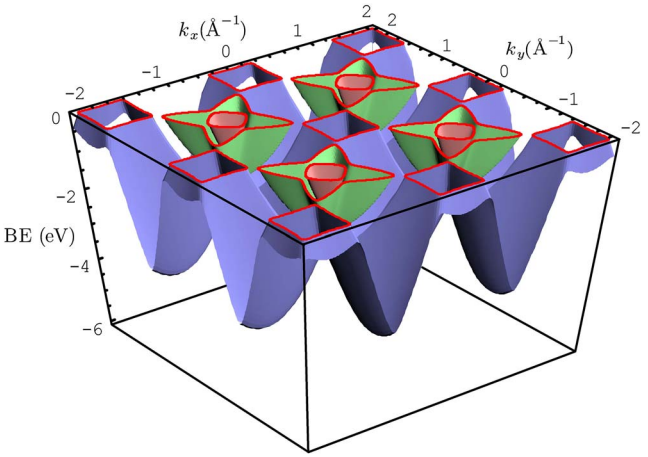

FIG. 5. (Color online) Schematic drawing of the dispersion of the surface band *S*, modeled as paraboloids repeated with $(\sqrt{2}\times\sqrt{2})R45°$ periodicity. Avoided-crossing gaps give rise to the formation of a three-contour Fermi surface. Contour No. 1 (blue) corresponds to the squares centered at $\bar{\Gamma}$ and $\bar{M}$ points. Contour No. 2 (green) are the stars, centered at $\bar{X}$ points. Contour No. 3 (red) are the squares also centered at $\bar{X}$ points.

experimental data are superimposed and are in very good agreement with the simple description provided by this model. Note that the contour close to normal emission is not observed in the experiment, due to its surface character, and the lack of band gap in this reciprocal space location. The intensity distribution at the Fermi energy is well reproduced by a $(\sqrt{2}\times\sqrt{2})R45°$ periodicity, which differs from the real $3\sqrt{2}$ symmetry of the surface. This is explained in part from the two-domain nature of the $3\sqrt{2}$ reconstruction. Due to the two domains present, the band gap that opens at the $3\sqrt{2}$ zone edges is detected in the Fermi surface only as an intensity decrease.

Figure 5 shows an energy vs momentum schematic drawing representing the dispersion of *S* in the repeated zone scheme. A paraboloid following the dispersion of the surface band *S* is repeated in reciprocal space with the $(\sqrt{2}\times\sqrt{2})R45°$ periodicity. Gaps open due to the effect of weak potentials in the reciprocal space areas where the Brillouin zone edges intersect. Due to this effect, the two-dimensional Fermi surface has three unconnected contours (equivalent to sheets in a three-dimensional Fermi surface). Each surface band giving rise to a contour is shown with a different color in Fig. 5. The first contour has a square shape and is centered at $\bar{M}$ points and (due to symmetry folding) at $\bar{\Gamma}$ points as well (see also Fig. 4). As shown in Fig. 5, this contour is traced back to the Fermi energy crossing of the blue band. The second contour is centered at $\bar{X}$ points, and has a four-point star shape (crossing of the green band). The third contour is also centered at $\bar{X}$ points and corresponds to a small electron pocket (red band). The topology of the three contours is probed in detail in Figs. 6 and 7. Figure 6 shows BE vs parallel momentum gray scale images for a series of azimuthal angles covering the first and second Fermi contours. The three top images in Fig. 6 correspond to the first contour around $\bar{M}$ points. The two bands are due to the two domains in the $3\sqrt{2}$ reconstruction. The upper band follows the Fermi contour. The gap due to the backfolding of the lower band decreases as the azimuthal angle increases and the nesting condition is worse satisfied.[20] The three bottom images in Fig. 6 correspond to the second Fermi contour. Note that for 22°, two Fermi energy crossings are detected, reflecting the two sides of the second contour. An avoided-crossing band gap is observed for 0.8 eV BE, separating the first and second bands. For larger angles, the gap appears at deeper BEs and the distance between the two sides of the contour increases. This behavior agrees well with the model shown in Fig. 4.

Figure 7 shows the behavior of the electronic bands along the $\bar{\Gamma}\bar{X}$ direction in the region around the $\bar{X}$ point. The narrow angular range selected is also shown in Fig. 4 as a white

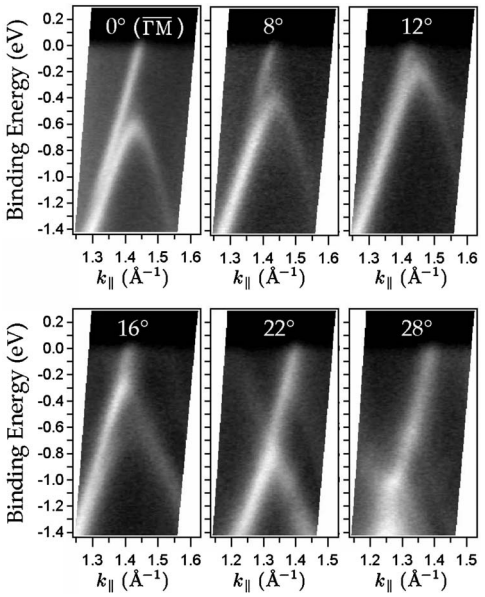

FIG. 6. Valence band structure for selected azimuthal angles with respect to the $\overline{\Gamma M}$ direction. The three top (bottom) images correspond to the angular range of the third (second) Fermi contour, as labeled in Fig. 5. The angular ranges probed in these images are shown as white lines in Fig. 4. See text for details.

line. This range probes the third Fermi contour, corresponding to the small electron pocket around the $\bar{X}$ point. The data shown in Fig. 7 are measured using a photon energy of $h\nu$=21.2 eV in order to enhance the intensity of the electron pocket band. The most intense peak observed in Fig. 7 corresponds to the bulk *sp* band, which disperses toward lower BEs as the parallel momentum increases. The electron pocket band is the small peak observed beyond the $\bar{X}$ point. It disperses toward the Fermi energy and it crosses it for $k_\parallel$=1.42 Å^{-1}, forming the third Fermi contour in Fig. 5. The second band (green in Fig. 5) is also detected around the $\bar{X}$ point as a peak with a BE around 1.9 eV.

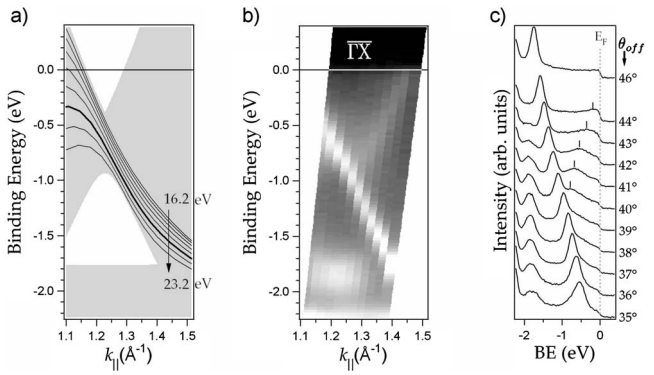

FIG. 7. (a) Calculated dispersion of the Cu *sp* bulk band along $\overline{\Gamma X}$ for different photon energies from 16.2 up to 23.2 eV in 1 eV steps (thick line: 21.2 eV) (Ref. 27). The shadowed area corresponds to the projection of the bulk bands. [(b) and (c)] Valence band structure in gray scale (b) and as energy distribution curves (c) for $h\nu$=21.2 eV along the $\overline{\Gamma X}$ direction in the region of the $\bar{X}$ point. See text for details.

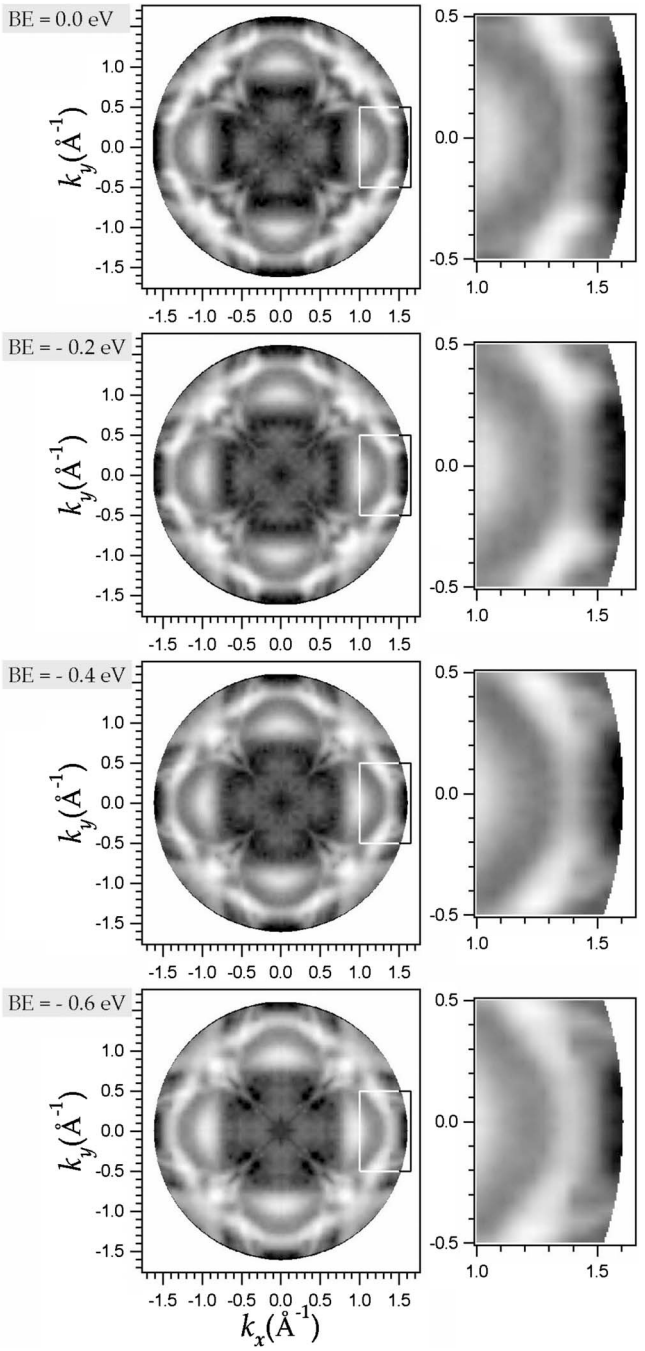

FIG. 8. Logarithm of photoemission intensity (integrated in a window of 25 meV width) vs parallel momentum, measured with $h\nu$=27 eV for Sn/Cu(100)-($3\sqrt{2}$). Constant binding energy surfaces for BE=0.0 (Fermi surface), −0.2, −0.4, and −0.6 eV are shown in the left column. The rectangular areas marked in the left column are shown in a larger scale in the right column.

Figure 8 shows the Fermi surface and constant energy surfaces for BEs down to −0.6 eV for the $3\sqrt{2}$ reconstruction. The right column shows an enlarged view of the reciprocal space area where the $3\sqrt{2}$ nesting is observed. The features observed in the constant energy surfaces agree well with the model used to draw Fig. 5. For instance, all contours (first, second, and third) become smaller as the BE increases. The evolution of the nesting area can be analyzed from the

detailed views in the right column. Due to the two domains present at the surface, a surface band always crosses the Fermi energy, and an absolute gap is not observed. However, the gapped area is detected as an arc with weaker intensity for $|k_y| \leq 0.4$ Å^{-1}. This arc with weaker intensity becomes smaller as the BE increases, to disappear completely for BE=−0.6 eV.

IV. DISCUSSION

Our above angle-resolved photoemission spectroscopy experiments bring a deeper knowledge and understanding about the properties of Sn/Cu(100)-$3\sqrt{2}$). This phase exhibits a quasi-free-electron-like surface state band with very different dispersion behaviors at high ($T > 360$ K) and low ($T < 360$ K) temperatures. The Fermi contour observed in the high-temperature phase is suppressed in the low-temperature phase along significant portions of reciprocal space, connected by a $2k_F$ nesting vector, which coincides very precisely with the periodicity of the low-temperature phase. Thus, a momentum dependent band gap opens in the low-temperature phase. The gap size is largest along the nesting direction, while it becomes smaller away from this direction. All these features suggest that the electronic energy plays an important role in the phase transition and agree well with a Peierls transition. An analysis of the value of the gap[20] indicates that the system is in the strong limit of the electron-phonon coupling[5,10,32–34] responsible for the instability.[35] In a conventional description of this limit, the gap survives up to a temperature T_0 much larger than the critical temperature T_c. In the range $T_c < T < T_0$, fluctuations destroy the long range order, but there is still enough local coherence to observe the gap, as the process is of order-disorder type. Only above T_0 the structural change is completed. In the case of Sn/Cu(100), the gap becomes zero only ~40 K above T_c, which is a fairly low value and indicates that the electronic energy win is involved in the phase transition, as expected in the weak-coupling limit case. We find an apparently contradictory behavior, as most features of the phase transition are typical of the strong-coupling limit. In a recent paper, Aruga[13] had proposed a new paradigm to classify 2D CDW systems, taking into account not only the gap size, but also the CDW correlation length ξ_{CDW}. If we estimate this magnitude from the range in reciprocal space where a band gap opens ($\Delta k \simeq 0.1$ Å^{-1}), we get $\xi_{CDW} = 2\pi/\Delta k \simeq 60$ Å. It is important to point out that ξ_{CDW} is different from the structural correlation length ξ, found, for instance, from the width of a surface diffraction peak.[20] ξ is referred to the long range structural correlation (domain size), while ξ_{CDW} measures the size of the wave packets.[13] At low temperature, $\xi > \xi_{CDW}$, and the gap is large. As temperature increases, ξ becomes smaller and eventually is comparable to ξ_{CDW}. Then, the spatial distribution of wave packets is effectively limited by ξ instead of ξ_{CDW}. Finally, ξ becomes so small that the gap disappears. Thus, whenever ξ_{CDW} is large, the gap closing takes place at a temperature T_0 much smaller than the value predicted by the mean field theory, due to the fact that ξ becomes comparable to ξ_{CDW} much before [in the case of Sn/Cu(100) only 40 K above T_c]. In the case of a large gap, but much smaller ξ_{CDW}, then a much larger temperature is required to get that ξ is comparable to ξ_{CDW}, and the observed behavior is well described within the strong-coupling limit. In the case of Sn/Cu(100) and also In/Cu(100),[13] the large gap indicates a strong coupling, but the concomitant large value of ξ_{CDW} governs the temperature dependence, which is similar to the weak-coupling case. These systems configure a range of physical systems, where large gaps are observed at the same time as large ξ_{CDW}.

ACKNOWLEDGMENTS

We acknowledge financial support by the Spanish MEC (FIS2005-00747) and by CAM (S-0505/PPQ/0316). The work at Elettra is supported by the EU under Contract No. RII3-CT-2004-506008 (IA-SFS).

[1] M. Potthoff, Adv. Solid State Phys. **42**, 121 (2002).
[2] G. Sambandamurthy, L. W. Engel, A. Johansson, E. Peled, and D. Shahar, Phys. Rev. Lett. **94**, 017003 (2005).
[3] A. V. Bune, V. M. Fridkin, S. Ducharme, L. M. Blinov, S. P. Palto, A. V. Sorokin, S. G. Yudin, and A. Zlatkin, Nature (London) **391**, 874 (1998).
[4] A. J. Berlinski, Rep. Prog. Phys. **42**, 1243 (1979).
[5] G. Grüner, *Density Waves in Solids* (Addison-Wesley, Reading, MA, 1994).
[6] K. Swamy, A. Menzel, R. Beer, and E. Bertel, Phys. Rev. Lett. **86**, 1299 (2001).
[7] H. W. Yeom, S. Takeda, E. Rotenberg, I. Matsuda, K. Horikoshi, J. Schaefer, C. M. Lee, S. D. Kevan, T. Ohta, T. Nagao, and S. Hasegawa, Phys. Rev. Lett. **82**, 4898 (1999).
[8] F. Schiller, J. Cordón, D. Vyalikh, A. Rubio, and J. E. Ortega, Phys. Rev. Lett. **94**, 016103 (2005).
[9] R. H. Friend and D. Jérome, J. Phys. C **12**, 1441 (1979).
[10] E. Tosatti, *Electronic Surface and Interface States on Metallic Systems*, edited by E. Bertel and M. Donath (World Scientific, Singapore, 1995); E. Tosatti, Festkoerperprobleme **15**, 113 (1975).
[11] J. M. Carpinelli, H. H. Weitering, E. W. Plummer, and R. Stumpf, Nature (London) **381**, 398 (1996).
[12] T. Aruga, J. Phys.: Condens. Matter **14**, 8393 (2002).
[13] T. Aruga, Surf. Sci. Rep. **61**, 283 (2006).
[14] C. Binns and C. Norris, J. Phys.: Condens. Matter **3**, 5425 (1991); C. Binns, M. G. Barthès-Labrousse, and C. Norris, J. Phys. C **17**, 1465 (1984).
[15] T. Nakagawa, G. I. Boishin, H. Fujioka, H. W. Yeom, I. Matsuda, N. Takagi, M. Nishijima, and T. Aruga, Phys. Rev. Lett. **86**, 854 (2001).
[16] T. Nakagawa, S. Mitsushima, H. Okuyama, M. Nishijima, and T. Aruga, Phys. Rev. B **66**, 085402 (2002).
[17] S. Hatta, H. Okuyama, M. Nishijima, and T. Aruga, Phys. Rev. B

71, 041401(R) (2005).
[18] S. Hatta, H. Okuyama, T. Aruga, and O. Sakata, Phys. Rev. B **72**, 081406(R) (2005).
[19] T. Nakagawa, H. W. Yeom, E. Rotenberg, B. Krenzer, S. D. Kevan, H. Okuyama, M. Nishijima, and T. Aruga, Phys. Rev. B **73**, 075407 (2006).
[20] J. Martínez-Blanco, V. Joco, H. Ascolani, A. Tejeda, C. Quirós, G. Panaccione, T. Balasubramanian, P. Segovia, and E. G. Michel, Phys. Rev. B **72**, 041401(R) (2005).
[21] G. Argile and G. E. Rhead, Thin Solid Films **87**, 265 (1982).
[22] G. E. Rhead, C. Argile, and M.-G. Barthes, Surf. Interface Anal. **3**, 165 (1981).
[23] G. Argile and G. E. Rhead, Surf. Sci. **135**, 18 (1983).
[24] E. McLoughlin, A. A. Cafolla, E. AlShamaileh, and C. J. Barnes, Surf. Sci. **482-485**, 1431 (2001).
[25] J. Martínez-Blanco, V. Joco, P. Segovia, T. Balasubramanian, and E. G. Michel, Appl. Surf. Sci. **252**, 5331 (2006).
[26] Y. Nara, K. Yaji, T. Iimori, K. Nakatsuji, and F. Komori, Surf. Sci. **601**, 5170 (2007).
[27] V. Joco, N. Mikuszeit, J. Martinez-Blanco, and E. G. Michel (unpublished).
[28] R. Courths and S. Hüfner, Phys. Rep. **112**, 53 (1984).
[29] P. Thiry, Ph.D. thesis, Universite Pierre et Marie Curie, 1981.
[30] M. Lindroos and A. Bansil, Phys. Rev. Lett. **77**, 2985 (1996).
[31] S. D. Kevan, Phys. Rev. B **28**, 2268 (1983).
[32] W. L. McMillan, Phys. Rev. B **16**, 643 (1977).
[33] C. M. Varma and A. L. Simons, Phys. Rev. Lett. **51**, 138 (1983).
[34] A. Fournel, J. P. Sorbier, M. Konczykowski, and P. Monceau, Phys. Rev. Lett. **57**, 2199 (1986).
[35] The electronic entropy is dominated by the distance between the upper band minimum and the Fermi energy, which we expect to be smaller than half of the gap. At variance with the case of In/Cu(100)-$c(4\times4)$ (Ref. 17), this parameter could not be estimated for Sn/Cu(100) due to the two domains of the $3\sqrt{2}$ reconstruction and the presence of an additional metallic band crossing the Fermi energy.